BCAL **Calorimetry Response**

Z. Papandreou [a,b,*]

[a] *Department of Physics, University of Regina, Regina, SK, S4S 0A2, Canada*
[b] *Prairie Particle Physics Institute, Regina, SK, S4S 0A2, Canada*

Abstract

Analytical calculations of the effective A, Z, ρ of the Barrel Calorimeter of the GlueX Project are presented, based on the volume ratios of the materials in its composition. In addition, the resulting radiation length, shower profile development, Molière radius and critical energy are determined. Comparisons with the Review of Particle Physics numbers and those from other sources are shown, together with detailed explanations of the employed formulae. An overview of general calorimetry concepts, a description of the properties of sampling calorimeters and the expected energy and timing resolutions are also included.

Key words: shower evolution, critical energy, radiation length, scintillating fiber
PACS: 29.40.Vj

1 Introduction

The electro-magnetic barrel calorimeter (BCAL) for the GlueX Project [1–3] consists of alternating layers of thin (0.5 mm) lead sheets and 1-mm-diameter scintillating fibers (SciFi). The lead sheets are grooved after passing through a swaging machine. The fibers are glued in the resulting grooves by using an optical epoxy. The resulting matrix has a design fiber pitch of $1.35\,mm$ in the horizontal direction and 1.18 mm in the vertical. The BCAL is segmented into 48 modules and has a radiation length of $15.5X_0$, as will be shown below. This device is destined to be placed inside the bore of the GlueX 2-Tesla super-conducting solenoid.

* Author's e-mail: zisis@uregina.ca

2 PSG Matrix: Effective Numbers

As reviewed in a previous report [4], the effective mass and atomic numbers can be determined by the following equations:

$$A_{eff} = \sum_i p_i A_i, \quad Z_{eff} = \sum_i p_i Z_i \tag{1}$$

$$A_{mol} = \sum_i n_i A_i, \quad Z_{mol} = \sum_i n_i Z_i \tag{2}$$

$$p_i = \frac{n_i A_i}{A_{mol}} \tag{3}$$

where n_i represents that number of atoms of the ith component of the compound and p_i is the weight of each element in the compound. Alternatively, p_i can be expressed as follows:

$$p_i = \frac{\rho_i \cdot V_i}{\Sigma(\rho_i \cdot V_i)} \tag{4}$$

and this is the formalism used primarily in the calculations below.

In applying this set of equations to the determination of the effective numbers of the lead, scintillating fiber and optical epoxy (PSG) matrix, one needs the chemical formulae for the SciFi and glue, since these are compounds as well. The examination of the relevant parameters begins immediately below, starting with the SciFi.

2.1 Scintillating Fibers

The precise chemical composition and density of scintillating fibers vary somewhat based on the manufacturer. In this paper, the properties of product BCF-12 (blue scintillating fibers) from Bicron [1] will be discussed and compared to the RPP [5] standard values: $X_0 = 43.72$ cm and $\rho = 1.032$ g/cm^3.

2.1.1 Polystyrene

The scintillating fibers used in the BCAL are composed of a core of Polystyrene and two layers of PMMA (polymethylmethacrylate, $C_5H_8O_2$) cladding: the

[1] Bicron, Newbury, Ohio, http://www.detectors.saint-gobain.com/.

first from acrylic and the second from fluor-acrylic material, having thicknesses of 3% and 1% of the fiber's diameter.

Polystyrene is a polymer made from the monomer styrene, a liquid hydrocarbon that is commercially manufactured from petroleum by the chemical industry. At room temperature, polystyrene is normally a solid thermoplastic, but can be melted at higher temperature for molding or extrusion, then resolidified. Styrene is an aromatic monomer and polystyrene is an aromatic polymer. The chemical makeup of polystyrene is a long chain hydrocarbon with every other carbon connected to a Phenyl group (an aromatic ring similar to benzene [6]), as shown in Fig. 1. Its contracted chemical formula can be written as $-(C_6H_5CH - CH_2)$-n, or more simply as $-(C_8H_8)$-n. Using this formula and formulae 1-4, one obtains $A_{mol} = 104.16$, fraction by weight of $p_C = 0.922427$ and $p_H = 0.0775730$, $A_{eff} = 11.160$ and $Z_{eff} = 5.610$.

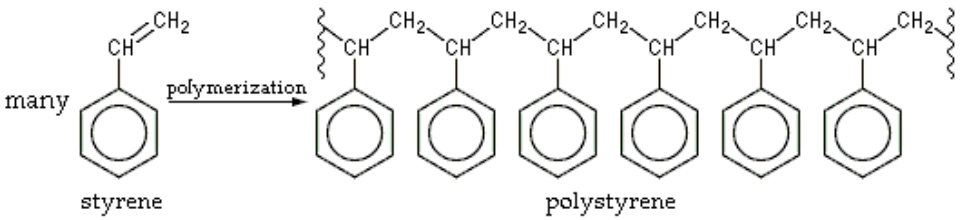

Fig. 1. Schematic of the Polystyrene polymer.

2.1.2 Bicron Scintillating Fibers

In its SciFi brochure [7], Bicron lists the number of *hydrogen* and *carbon* atoms per cc in the core as 4.82×10^{22} and 4.85×10^{22}, respectively. Using these in equations 2 and 3 results in $A_{mol} = 63.12$, and fraction by weight of $p_C = 0.92287$ and $p_H = 0.0730$. These numbers, in turn, yield $A_{eff} = 11.162$ and $Z_{eff} = 5.615$, using equation (1).

2.2 Bulk Scintillator

The chemical formula for bulk scintillator is C_8H_9. Use of the above formulae results in $A_{mol} = 105.17$, fraction by weight of $p_C = 0.9135685$ and $p_H = 0.0864315$, $A_{eff} = 11.059$ and $Z_{eff} = 5.568$ in perfect agreement with the values calculated by GEANT.

2.3 Summary

The volume ratio of lead:fibers:glue is **37** : **49** : **14**, based on measurements of the PSG matrix using a lab microscope [8]. The exact geometry is reflected in Table 1. Note that the vertical fiber pitch of 1.215 mm is larger than the design value of 1.18 mm, based on the KLOE calorimeter [9]. This implies a slightly smaller value of the total number of radiation lengths of the BCAL within its thickness of 22.5 cm. The horizontal pitch, a product of the groove-to-groove distance on the lead sheets, is exactly at the design value of 1.35 mm. A schematic of the PSG Matrix geometry is shown in Fig. 2.

Quantity	**Value**
Lead sheet thickness	0.5 mm
Fiber Diameter	1 mm
Horizontal Fiber Pitch	1.351 ± 0.004 mm
Vertical Fiber Pitch	1.215 ± 0.005 mm
Glue Box Height	0.233 ± 0.004 mm
Glue Ring Thickness	0.053 ± 0.003 mm

Table 1
Measured dimensions of the PSG Matrix.

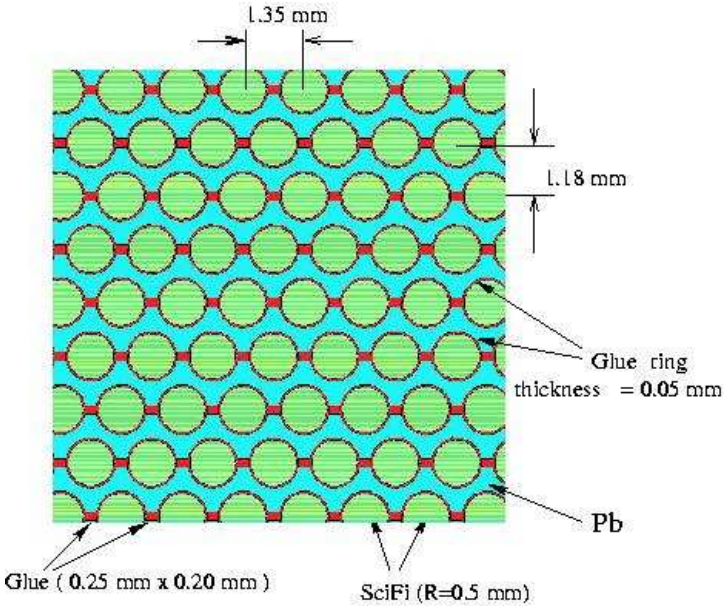

Fig. 2. PSG Matrix geometry. This is the standard geometry used in GEANT for the standalone Monte Carlo.

The chemical formulae[2] for the scintillating fibers and for the Bicron BC-

[2] As programmed by R. Hakobyan into the GEANT routine *ugeom.f.*

600 two-component optical epoxy are $C_{0.9213}H_{0.0773}N_{8.73\times10^{-4}}O_{5.03\times10^{-4}}$ and $C_{60}H_{79}N_2O_3$, respectively (for more detail see Table 2). The SciFi ratios in this table were calculated by GEANT.

The A, Z and proportion by weight of each element are given in Table 2. Clearly, the differences in A_{eff} and Z_{eff} among the four *scintillating* materials are insignificant. The effective A, Z, and densities of the sub-compounds are presented in Table 3. The A_{eff} and Z_{eff} in the latter table were calculated using equations (1), (2) and (4). A third use of these equations provides the final values for the PSG matrix listed in the last row of Table 3.

Element	**A**	**Z**	**Fraction by Weight**				
			Bulk	Polystyrene (C_8H_8)	Bicron SF	**SciFi**	**Glue**
H	1.01	1	0.0864	0.0776	0.0773	0.077	0.091
C	12.01	6	0.9136	0.9229	0.9224	0.921	0.822
N	14.01	7	-	-	-	0.001	0.032
O	16.00	8	-	-	-	0.001	0.055
	A_{eff}		11.059	11.160	11.162	11.163	11.291
		Z_{eff}	5.568	5.610	5.615	5.615	5.686

Table 2
Mass, atomic numbers and proportions by weight of the PbSciFi elements.

Compound or **Element**	ρ ($g\ cm^{-3}$)	A_{eff}	Z_{eff}	**Fraction by weight**
SciFi	1.049	11.163	5.615	0.105378
Glue	1.180	11.291	5.686	0.033861
Pb	11.35	207.2	82	0.860781
PbSciFi Matrix	**4.88**	**179.91**	**71.37**	

Table 3
Densities, effective A and Z and proportion by weight of the PbSciFi compounds.

3 Radiation Length Calculations

The dominant energy loss mechanism for photons in a calorimeter is the $\gamma \rightarrow e^+e^-$ reaction, via consecutive pair production and bremsstrahlung processes. The quantity that best characterizes the penetration depth of a photon shower is the radiation length, X_0. This quantity is expressed in units of cm or g/cm^2. The radiation length [5]:

- describes the mean distance over which a high energy electron loses all but 1/e of its energy ($E(x) = E_0 e^{-x/X_0}$);
- represents 7/9 of the mean free path for pair production by a high energy photon ($I(x) = I_0 e^{-7x/9X_0}$);
- is an appropriate scale for describing high energy electro-magnetic cascades; and
- is a scaling variable for the probability of occurrence of bremsstrahlung and pair production as well as for the variance of the angle of multiple scattering.

Four formulae can be used to determine X_0 (see references [10–13]). The second and third of these provide a clearer view of the functional dependence on Z, and they include screening effects of the nuclear field by the atomic electrons. The third equation is an approximation while the second a result of a compact fit to the data with an accuracy of better than 2.5% for all elements except He. The fourth one is identical to the first one and is used for convenience in EGS5 [13] and GEANT [14] Monte Carlo packages. (Note: GEANT effectively uses EGS5 in its innards).

$$\frac{1}{X_0} = 4\alpha r_e^2 \frac{N_A}{A} \left(Z^2 [L_{rad} - f(Z)] + Z L'_{rad} \right) \tag{5}$$

$$\frac{1}{X_0} = 4\alpha r_e^2 \frac{N_A}{A} \left(Z(Z+1) \ln \frac{287}{\sqrt{Z}} \right) \tag{6}$$

$$\frac{1}{X_0} = 4\alpha r_e^2 \frac{N_A}{A} \left(Z(Z+1) \ln \frac{183}{Z^{\frac{1}{3}}} \right) \tag{7}$$

$$\frac{1}{X_0} = 4\alpha r_e^2 \frac{N_A}{A} Z(Z + \xi(Z)) \left(\ln \frac{183}{Z^{\frac{1}{3}}} - f(Z) \right) \tag{8}$$

where

$$\xi(Z) = \frac{L'_{rad}}{L_{rad} - f(Z)} \tag{9}$$

For $A = 1$ gmol^{-1} we obtain $4\alpha r_e^2 \frac{N_A}{A} = (716.408 \text{ gcm}^{-2})^{-1}$, where $N_A = 6.022 \times 10^{23}$ mol^{-1} and the quantity $r_e = \frac{1}{4\pi\epsilon_0} \frac{e^2}{mc^2}$ represents the classical electron radius, equal to 2.818×10^{-13} cm.

The function $f(Z)$,

$$f(Z) \approx a^2 \left[(1 + a^2)^{-1} + 0.20206 - 0.0369 a^2 + 0.0083 a^4 - 0.002 a^6 \right] \tag{10}$$

represents the bremsstrahlung and pair production Coulomb correction for element Z and is an infinite sum, but for elements up to uranium it is accurate

to four significant figures. In this equation $a = \alpha Z$ [15] and $\alpha = \frac{1}{137}$. The functional dependence of f on Z is illustrated in Fig. 3.

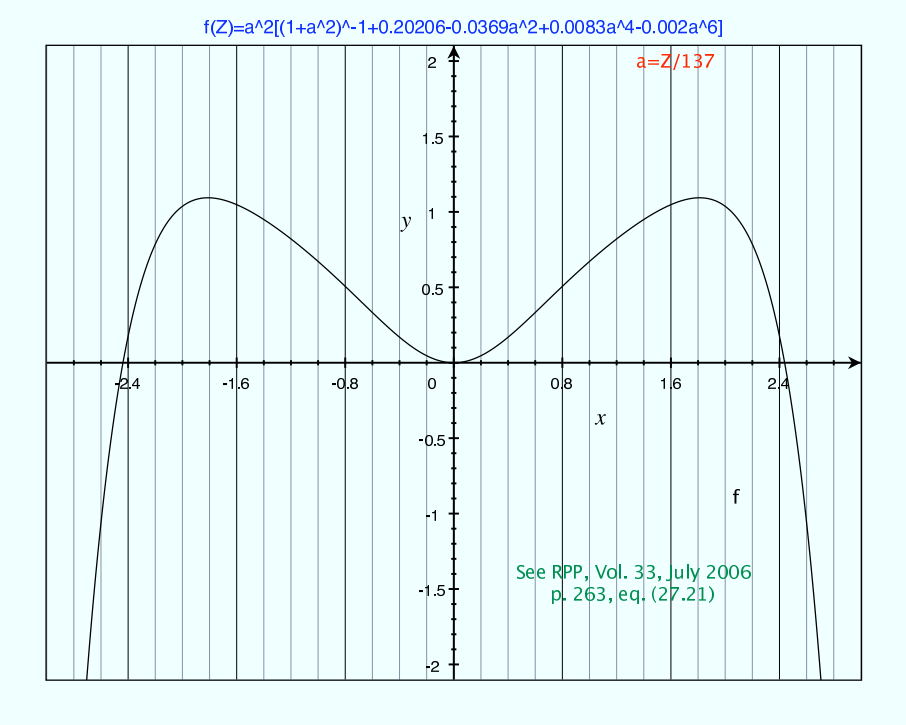

Fig. 3. Coulomb correction function for element Z due to bremsstrahlung and pair production.

For $Z > 4$ we have $L_{rad} = \ln\left(184.15Z^{-\frac{1}{3}}\right)$ and $L'_{rad} = \ln\left(1194Z^{-\frac{2}{3}}\right)$. These parametric forms are used in EGS5 for $Z > 4$; otherwise the values tabulated in Table 4 are used [13].

Z	L_{rad}	L'_{rad}
1	5.310	6.144
2	4.790	5.621
3	4.740	5.805
4	4.710	5.924
>4	$\ln\left(184.15Z^{-\frac{1}{3}}\right)$	$\ln\left(1194Z^{-\frac{2}{3}}\right)$

Table 4
Tabulated valued for L_{rad} and L'_{rad} in EGS5.

All three X_0 equations (5)-(7) were entered into the *Grapher* application [16] on an iMac. This package plots the function and evaluates it at any point. The results are shown in Table 5.

Using the PSG numbers from Table 3 and formulae (5)-(7) one obtains the results in in Table 6. Alternatively, the X_0 for the PSG matrix can also be

Formula		**Al**	**Pb**	**Bulk**	**SciFi**	**Glue**	**PSG Matrix**
	A	26.980	207.2	11.059	11.163	11.291	179.91
	Z	13	82	5.568	5.615	5.686	71.37
	ρ	2.7	11.35	1.032	1.049	1.180	4.88
5	X_0	24.01	6.37	44.74	44.54	44.08	7.06
	(cm)	8.89	0.56	43.35	42.46	37.36	1.45
6	X_0	24.26	6.31	45.10	44.89	44.42	7.08
	(cm)	8.99	0.56	43.70	42.79	37.64	1.45
7	X_0	24.39	5.83	46.69	46.46	45.95	6.59
	(cm)	9.03	0.51	45.24	44.29	38.94	1.35
GEANT	(cm)	8.9	0.56	42.1	41.4	36.3	N/A

Table 5
Radiation length of several materials, calculated via the Grapher application [16]. The A, Z and ρ for each calculation are shown as well. The X_0 is shown in units of g/cm^2 on one line and immediately below in cm. The results using all three formulae are in close agreement, with equation (7) deviating from equation (5) by 2%, 7% and 8.5% for Al, PSG Matrix and Pb, respectively.

Formula	X_0 $(g\ cm^{-2})$	X_0 (cm)	$n = \frac{d}{X_0}$ with 1" Al	$n = \frac{d}{X_0}$ with $\frac{3}{4}$" Al
5	7.06	1.45	15.5	16.4
6	7.08	1.45	15.5	16.4
7	6.59	1.35	16.6	17.6

Table 6
Radiation length of PbSciFi matrix and number of radiation lengths contained in the full thickness of the BCAL.

calculated via the following equation:

$$\frac{1}{X_0} = \Sigma \frac{w_j}{X_j} \tag{11}$$

where w_j and X_j are the fraction by weight and the radiation length of the jth element. This was done and the results were identical to the use of equations (5)-(7) with the A_{eff} and Z_{eff} numbers, as expected.

The full thickness of the BCAL in Table 6, d, is equal to 25 cm minus the thickness of the aluminum backing plate. For the latter, two values are assumed: 1" (design value) and $\frac{3}{4}$" (minimum thickness for structural rigidity). The prototype 4-m-long (full-sized) module has a 1" Al plate.

4 Critical Energy

The next parameter of interest for an electro-magnetic calorimeter is the critical energy, E_c, whose definition is based on the energy loss mechanism of electrons. An electron loses energy in two ways:

- Bremsstrahlung, at a rate approximately proportional to its energy, and
- Ionization loss, at a rate that changes logarithmically with its energy.

There are two definitions of the critical energy: Berger and Seltzer [17] define E_c where the energy lost due to ionization becomes approximately equal to that lost due to the bremmstrahlung process; Rossi [18] defines it where the ionization loss per radiation length becomes equal to the electron energy. The functional dependence of E_c on Z for the two methods is expressed as follows, and is shown graphically in Fig. 4. A comparison of the two methods is illustrated in Fig. 5.

$$E_c = \frac{800 \text{ MeV}}{Z + 1.2} \tag{12}$$

$$E_c = \frac{610 \text{ MeV}}{Z + 1.24} \tag{13}$$

which give $E_c = 11.02$, 8.36 MeV, respectively, for $Z = 71.37$ (the effective atomic number of our PSG Matrix; see Table 5). This quantity is needed for the calculation of the longitudinal and lateral (transverse) shower evolution.

5 Electromagnetic Cascades

A high-energy electron (or photon) impinging on a material with sufficient thickness (in terms of radiation length) and effective Z produces an electromagnetic cascade via the processes of pair production and bremsstrahlung. A parent electron (or photon) will radiate photons (convert to pairs), which radiate and produce fresh pairs in turn, the number of particles increasing exponentially with depth. Electron energies eventually fall below E_c, and then dissipate their energy by ionization and excitation rather than by bremsstrahlung. In describing shower behavior, it is convenient to use two scale variables, $t = x/X_0$ and $y = E/E_c$, so that depth in the material is described in units of radiation length and energy in units of critical energy.

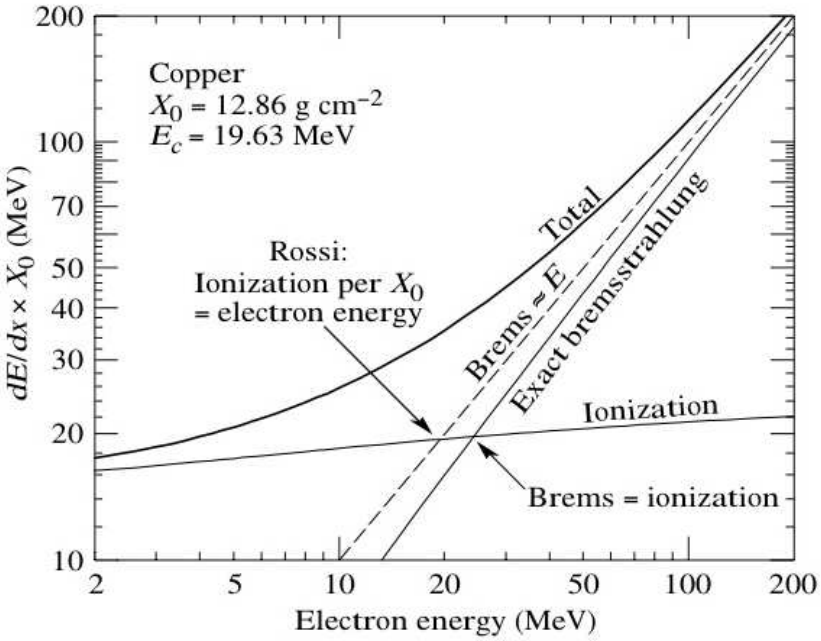

Fig. 4. Critical Energy definition [5].

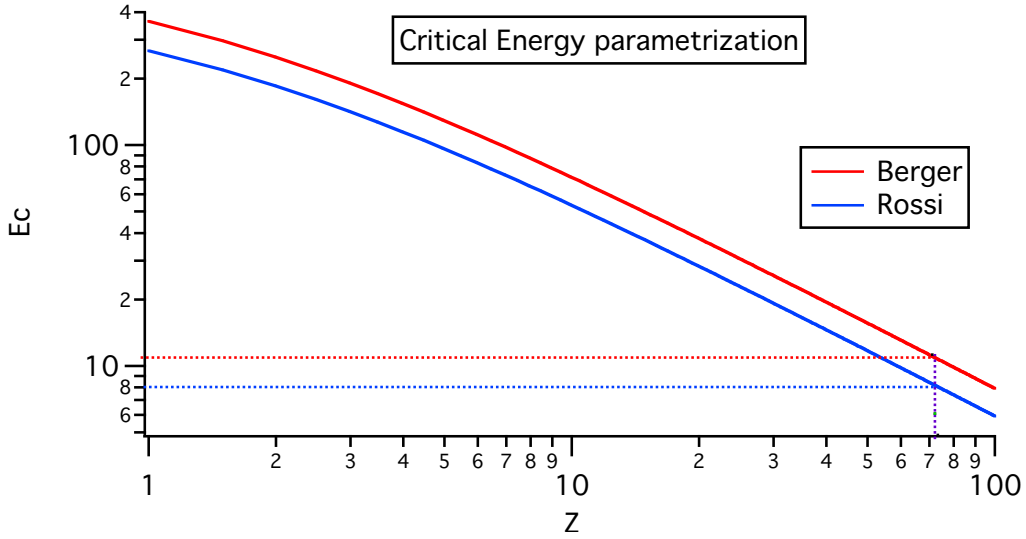

Fig. 5. Critical energy parametrization.

5.1 Longitudinal Shower Development

The longitudinal development of an electromagnetic cascade depends on the high-energy part of the cascade, and therefore scales with the radiation length in the material. The mean longitudinal profile of the energy deposition of an

electromagnetic cascade is expressed as:

$$\frac{dE}{dt} = E_0 b \frac{(bt)^{a-1} e^{-bt}}{\Gamma(a)} \tag{14}$$

where E_0 is the incident particle energy, $t = x/X_0$ is the depth inside the material, and a and b are parameters related to the nature of the incident particle ($e^{\pm}$ or γ). The shower maximum (depth at which the largest number of secondary particles is produced) can be easily shown to be:

$$t_{max} = (a-1)/b = lny + t_0 = ln\frac{E_0}{E_c} + t_0 \tag{15}$$

where t_0 is -0.5 for electrons and $+0.5$ for photons. The parameter b is assumed to be ≈ 0.5 (see Fig. 6 for more details). Finally, the calorimeter thickness that contains 95% of the shower energy can be written as:

$$t_{95\%} \approx t_{max} + 0.08Z + 9.6 \tag{16}$$

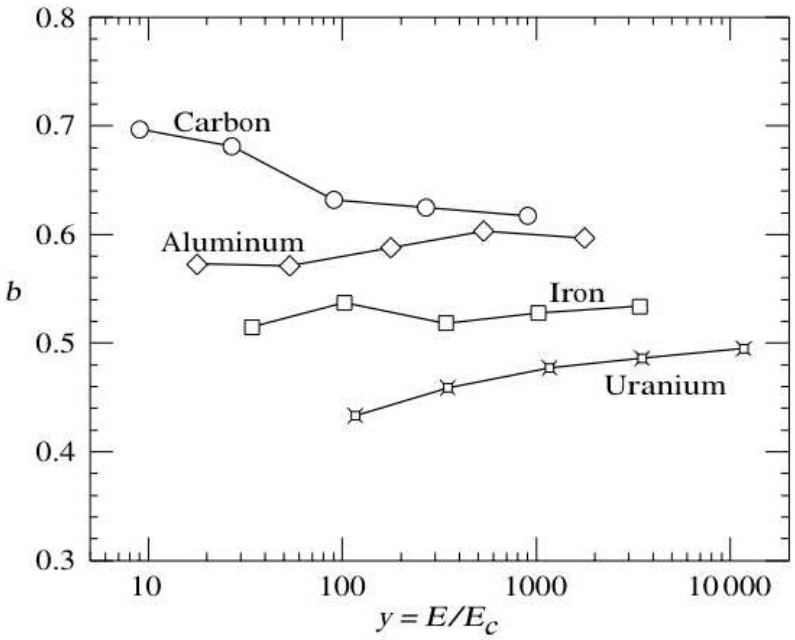

Fig. 6. Fitted values of the electromagnetic cascade scale parameter b [5].

Representative values of t_{max} are presented in Table 7. A 1 GeV photon results in $t_{95\%}$ equal to $20.3X_0$ and $20.6X_0$ using equations (12) and (13), respectively. The evolution of t_{max} and $t_{95\%}$ with incident photon energy is shown in Fig. 7.

Finally, the longitudinal shower profile was determined using the analysis and graphing package *IGOR Pro* [19], following equation (14). The results for a

E_0 (MeV)	t_{max} [Eq. (12)] (units of X_0)	t_{max} [Eq. (13)] (units of X_0)
40	1.79	2.06
100	2.71	2.98
150	3.11	3.38
250	3.62	3.89
500	4.32	4.59
650	4.58	4.85
1000	5.01	5.28
2000	5.70	5.97

Table 7
Representative values of t_{max} using equations (12) and (13), respectively. To compute $t_{95\%}$ simply add 15.31 to the tabulated values.

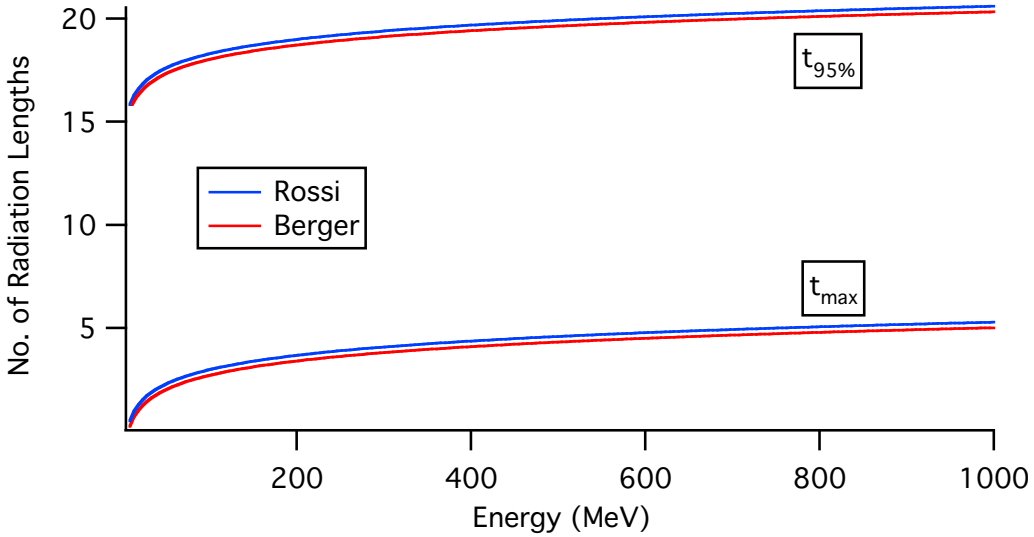

Fig. 7. Evolution of t_{max} and $t_{95\%}$ with incident photon energy for the two parametrizations in equations (12) and (13).

number of incident photon energies are shown in Fig. 8: 40 MeV corresponds to the BCAL's expected threshold, 150 MeV and 650 MeV are the lower and upper limit of the tagged photon spectrum in the September 2006 beam tests at Hall-B/JLab, and 1 GeV and 2 GeV are shown for general interest. As the energy of the incident photon drops, the shower peaks at lower number of radiation lengths and a higher percentage of the shower is contained within the $15.5X_0$ of the BCAL (indicated by the arrow in the graph), as demonstrated by the areas under the curves. Indeed, at $25X_0$ nearly all of the shower is contained, as mentioned above, even for 2 GeV photons.

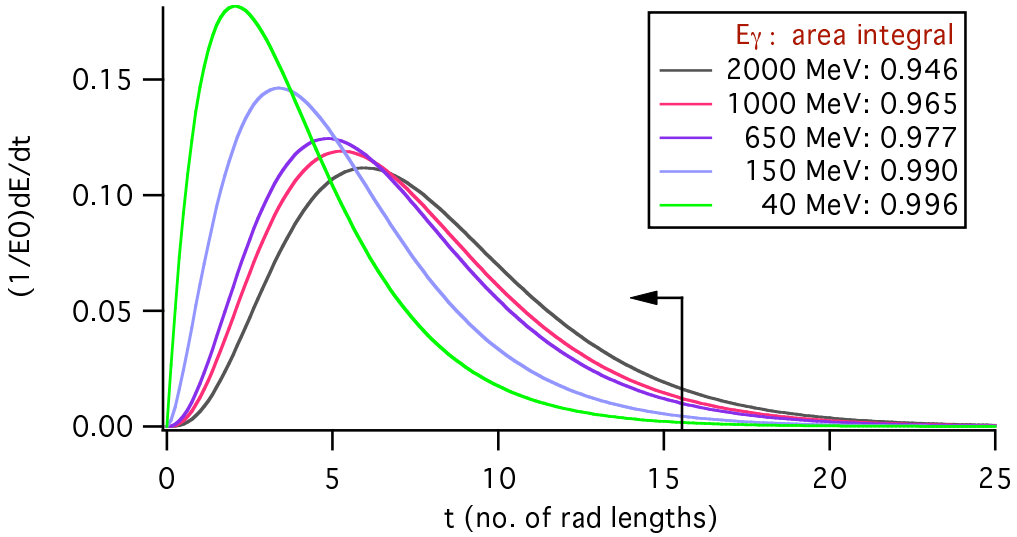

Fig. 8. Longitudinal shower development.

It should be noted that for calorimeters with $\sim 25X_0$ the longitudinal shower leakage out the rear is $< 1\%$ for e^- energies of up to 300 GeV. For the BCAL, using the 1" Aluminum plate, Monte Carlo simulations for showers at normal incidence [20,21] have shown an energy leakage from the rear of the calorimeter of 3.4% at 650 MeV and 2 % at 200 MeV, in qualitative agreement with the analytical predictions of Fig. 8. A typical simulated depth profile is shown in Fig. 9, for 650 MeV incident photons.

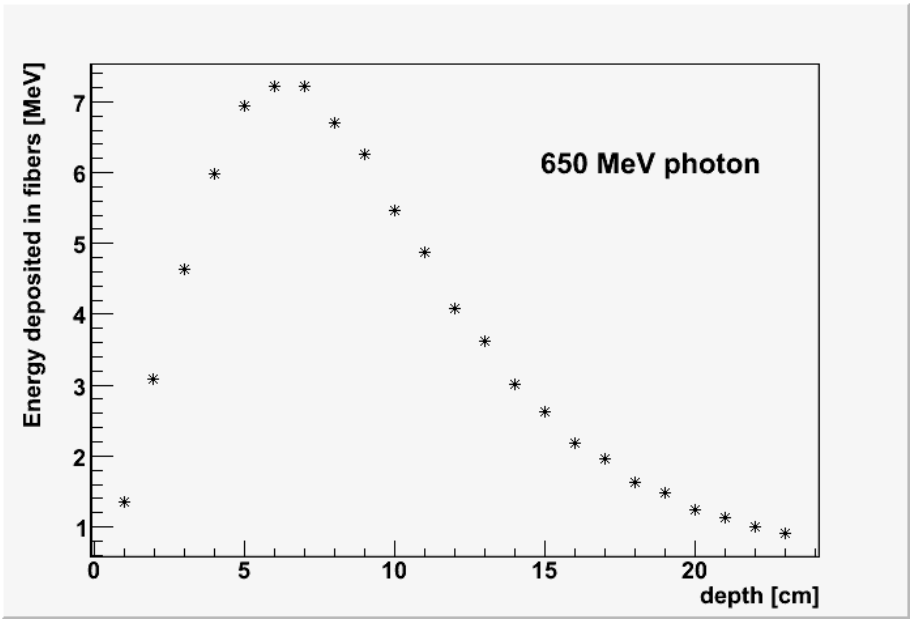

Fig. 9. Simulated shower depth profile for 650 MeV incident photons at $\theta = 90^o$ using the standalone Monte Carlo based on GEANT.

5.2 Lateral Shower Development

The transverse size of an electro-magnetic shower is mainly due to multiple scattering of electrons and positrons away from the shower axis. Bremsstrahlung photons emitted by these can contribute further to the spread.

A measurement of the transverse size, integrated over the full shower depth, is characterized by the Molière radius, R_M, which is given by:

$$R_M(\mathrm{g/cm^{-2}}) = E_s \frac{X_0(\mathrm{g/cm^{-2}})}{E_c\ (\mathrm{MeV})} \tag{17}$$

or

$$R_M(\mathrm{cm}) = E_s \frac{X_0(\mathrm{cm})}{E_c\ (\mathrm{MeV})} \tag{18}$$

and with $E_s \approx 21$ MeV (scale energy) and $E_c = 8.4$ MeV (using the Rossi parametrization) and the appropriate values for X_0 from Table 6 one obtains $R_M \approx 17.65$ g/cm^2 or $R_M \approx 3.63$ cm. In other words, 90% of the electromagnetic shower is contained in a cylinder of radius R_M and 99% of it in a cylinder of radius $3.5R_M$.

In a material containing a weight fraction w_j of an element with critical energy E_{cj} and radiation length X_j, the Molière radius is given by:

$$\frac{1}{R_M} = \frac{1}{E_s} \sum \frac{w_j E_{cj}}{X_j} \tag{19}$$

where the Rossi parametrization [18] is used. Employing equations (5), (13), (19) and values from Tables 3 and 5, the Molière radius is calculated to be $R_M \approx 16.54$ g/cm^2, about 6% off the value determined using the effective X_0 of the PSG matrix (see previous paragraph).

Detailed studies of the lateral spread have been done and Monte Carlo simulations have been shown to agree quite well with measurements [22]. The lateral profile has been demonstrated to follow the behavior of a combined exponential and Gaussian fit:

$$\frac{dE}{dA} = \frac{B_1}{r} e^{-r/\lambda_1} + \frac{B_2}{r} e^{-r^2/\lambda^2} \tag{20}$$

These two curves represent the non-electromagnetic and electromagnetic shower component, resepectively. The exponentially decreasing shower halo follows

the expectation for isotropically distributed shower particles interacting on average after one nuclear interaction length (λ_1), while the Gaussian core has a width of $\sim 2\, R_M$ [23].

5.3 Shower Multiplicity

The dramatic result of the combined phenomena of bremsstrahlung and pair production is the creation of shower cascades for high energy electrons and photons, as mentioned above. A simple model of assigning half the electron's energy to the produced pair, and so on, leads to $N = 2^t$ particles after t radiation lengths, with photons, electrons and positrons approximately equal in number. This simple models neglects ionization loss and the energy dependence of pair-production cross section; more accurate estimates can be obtained via Monte Carlo simulations. The number of particles at the shower maximum, the number exceeding a given energy and the total integral track length, L, of charged particles (in radiation lengths) are given by [12]:

$$N_{max} = exp[t_{max}\, ln\, 2] = \frac{E_0}{E_c} \tag{21}$$

$$N(> E) = \int_0^{t(E)} N dt = \int_0^{t(E)} e^{t\, ln\, 2} dt \simeq \frac{e^{t(e)\, ln\, 2}}{ln\, 2} = \frac{E_0/E}{ln\, 2} \tag{22}$$

$$L = \frac{2}{3} \int_0^{t_{max}} N dt = \frac{2}{3\, ln\, 2} \frac{E_0}{E_c} \simeq \frac{E_0}{E_c} \tag{23}$$

A represenative set of numbers is shown in Table 8. One observes that at eight radiation lengths the energy per particle, E_{pp}, for a 1 GeV incident photon drops to just under 4 MeV.

The development of a shower has the three main characteristics:

- The maximum is at a depth that increases logarithmically with E_0;
- The number of shower particles at maximum depth is proportional to E_0; and
- The total track-length integral is also proportional to E_0.

t (no rad lengths)	$N = 2^t$	$E_{pp} = 1000/N$ (MeV)
1	2	500
2	4	250
3	8	125
4	16	62.5
5	32	31.3
6	64	15.6
7	128	7.81
8	256	3.91
10	1024	0.98
15	32768	0.03

Table 8
Number of shower particles at shower maximum.

6 Electromagnetic Calorimeter Features

The discussion in this section will focus on sampling electromagnetic calorimetry. The formulae in preceding sections represent, approximately, the average shower behavior. However, since the physics behind pair production and bremsstrahlung is well understood, Monte Carlo simulations use these widely; the standards in particle physics are EGS [13] and GEANT [14].

6.1 Energy Resolution

The total track length of the shower, L, is defined as the sum of all ionization tracks due to all charged particles in the electromagnetic cascade, and can be expressed by equation (23). The intrinsic resolution of an ideal calorimeter, depends mainly on the fluctuations of L. Since L is proportional to the number of tracks in the shower, and the shower is a stochastic process, the intrinsic resolution is given by

$$\sigma(E) \sim \sqrt{L} \tag{24}$$

from which the well-known dependence on fractional energy resolution

$$\frac{\sigma(E)}{E} \sim \frac{1}{\sqrt{L}} \sim \frac{1}{\sqrt{E}} \tag{25}$$

can be derived [24]. The energy resolution of a calorimeter receives contributions from other effects, and its full form is:

$$\frac{\sigma_E}{E} = \frac{a}{\sqrt{E}} \oplus b \oplus \frac{c}{E} \tag{26}$$

where $\oplus$ denotes addition in quadrature. The three terms in this equation are described in the subsections below.

An alternative argument goes as follows. Tracks in a shower are not all created equal; some have very little and some have a lot of energy, so that the fluctuations in shower energy and particle number are weakly correlated. There is self-similarity (scaling) for why $\sigma(E)$ goes like $\sqrt{E}$ using the evident decomposition rule for showers that a large shower is made up of smaller ones, each of which is independent. Any branch of a shower with energy $E_1 < E_0$ can be split off and treated separately, with:

$$\sigma^2(E_0) = \sigma^2(E_1) + \sigma^2(E_0 - E_1) \tag{27}$$

where $\sigma^2(E)$ is the measurement variance for showers with incident energy E. Equation 27 is a self-similarity relation and is a a rigorous consequence of independence of the different branches of the shower. It holds for all E_1 on the interval $(0, E_0)$. This equation can be solved by noting that:

$$d/dE[\sigma^2(E) - \sigma^2(E_0 - E)] = 0 \tag{28}$$

The unique solution to Equation 28 is $\sigma^2(E) = E * C$, where C is constant, in agreement to the above reasoning.

6.1.1 Stochastic Term

Term a in Equation (26) is known as the *stochastic* term as it represents statistical fluctuations, such as intrinsic shower fluctuations, photoelectron statistics and sampling fluctuations; in addition, dead material in front of the calorimeter also contributes to this term.

Photoelectron statistics are the effect of variations in the detector readout's signal for a fixed energy deposit in the active material. For a well-designed sampling calorimeter, this effect is much smaller than the contribution due to sampling fluctuations. Good photoelectron statistics dominate the timing resolution and are very important near the detection threshold (40 MeV for the BCAL) and for low energy photons in conjunction to the noise [25]; optimal signal-to-noise ratio is desired.

In a sampling calorimeter, such as the BCAL, the energy deposited in the active medium (scintillating fibers) fluctuates event by event since the active layers are interleaved with Pb layers. These are the above mentioned sampling fluctuations and are the largest contribution to the energy resolution. They depend on variations of the number of charged particles, N_{ch}, which cross the scintillating fibers:

$$N_{ch} \sim \frac{E_0}{t} \tag{29}$$

where t is the thickness of the inactive layers in X_0 units. For statistically independent crossings of the active layers, the contribution to $\sigma(E)/E$ due to the sampling fluctuations is given by [26]:

$$\frac{\sigma(E)}{E} \sim \frac{1}{N_{ch}} \sim \sqrt{\frac{t}{E_0}} \tag{30}$$

Clearly, less absorber and more scintillating fiber thickness (i.e. larger *sampling fraction*) improves the energy resolution, at the expense of 'stopping power' (total thickness in number of radiation lengths) of the calorimeter due to the low detector density. For a sampling calorimeter to match the energy resolution of a homogeneous one, inactive thickness of a few percent is needed, which is impractical. Moreover, a low calorimeter density implies that the showers need more space to develop in all directions thus resulting in overlapping clusters and impeding the particle identification process, and it also results in an increase of the e/h value of the calorimeter which degrades its 'compensation' capability towards detection of hadrons. A second way of reducing sampling fluctuations is to increase the *sampling frequency*, which is depends on the number of independent sampling layers for a fixed sampling fraction. This can be achieved by reducing the scintillating fiber diameter while introducing more layers to keep the sampling fraction constant.

In order to understand these two effects on the energy resolution, recall that the energy of a showering photon or electron is primarily deposited in the inactive material (Pb for the BCAL) via a very large number of 'soft' electrons [23]. These secondary electrons have average energies much lower than the critical energy of the material and an effective range that is much less than the inter-layer distance. For the BCAL, the atomic number of the inactive material ($Z = 82$) is much larger than that of the active material ($Z = 5.615$) so the overwhelming majority of these soft electrons are produced and absorbed in the inactive material, because of the Z-dependence of Compton scattering and the photoelectric effect [27].

Most of these electrons will not contribute to the calorimeter's signal; the sampling fluctuations come from those that *do* contribute. This number can

be increased by increasing the total surface of the boundary between active and inactive layers, which can be achieved by either increasing the sampling fraction or sampling frequency. However, such increases result in modest gains in resolution: for example, reducing the fiber diameter from $1.0\,mm$ to $0.5\,mm$ results in four times as many fibers per unit volume, yet the energy resolution improves only by a factor of $\sqrt{2}$. In other words, the resolution scales with the fourth root of the number of fibers. This has significant implications in cost and manpower for handling and construction.

The sampling fraction is indeed an important parameter of sampling calorimeters, and can be expressed as:

$$f_{samp} = \frac{E_{mip}(active)}{E_{mip}(active) + E_{mip}(inactive)} \tag{31}$$

It should be noted that this quantity impacts the noise term of the energy resolution [24], a point that will be discussed further in Section 6.1.3. For a fixed number of X_0 in the BCAL, the coefficient of the stochastic term of the energy resolution is approximately equal to $6\sqrt{t/f}$ %, where t is the inactive plate thickness (0.089) and f the sampling fraction (0.12) [28], resulting in $a \simeq 5\%$ for the BCAL [29]. The contribution of the sampling fluctuations has been simulated and shown in Figs. 10 and 11.

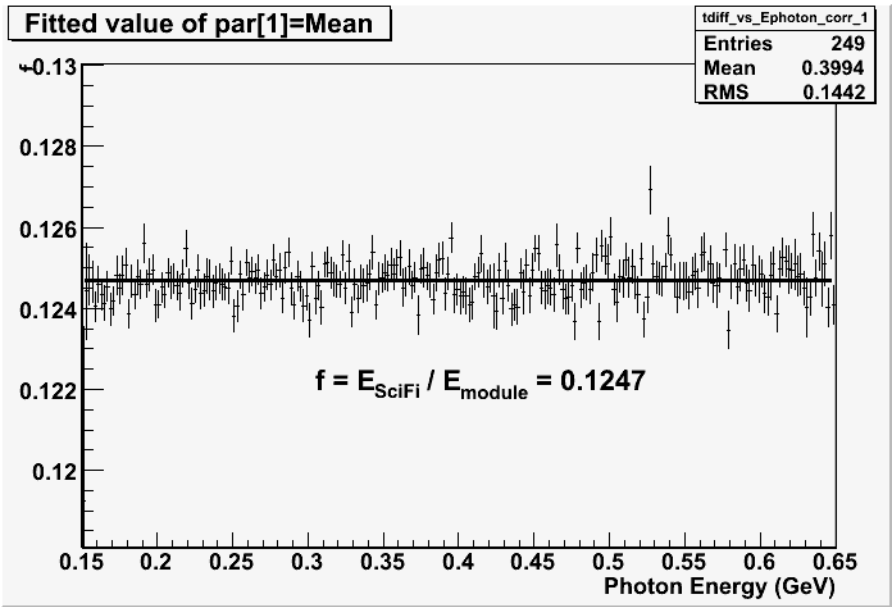

Fig. 10. Simulation of the BCAL sampling fraction as a function of tagged photon energy, corresponding to the Fall 2006 Beam Test at Hall-B/Jefferson Lab [28].

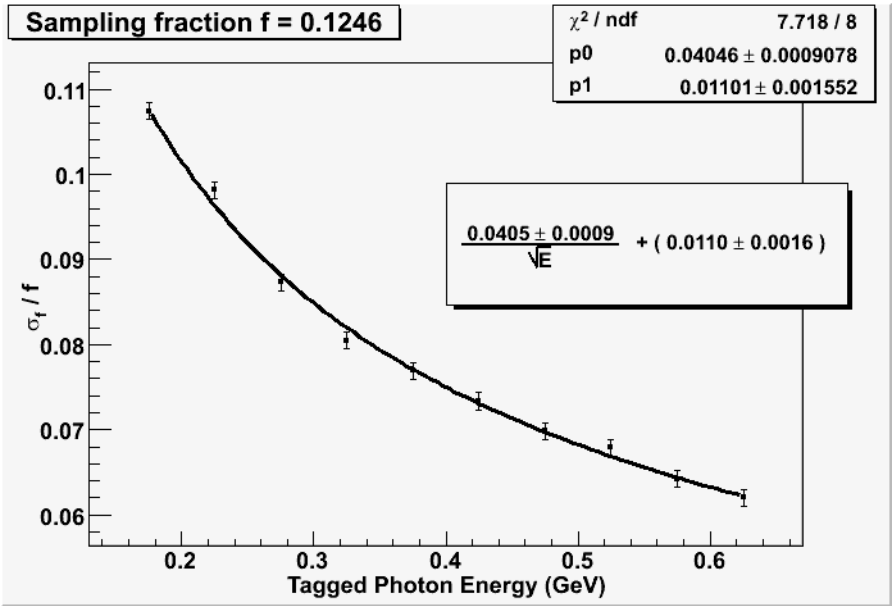

Fig. 11. Simulation of the BCAL sampling fraction resolution [28].

6.1.2 Floor Term

Term b in Eq. (26) is known as the *systematic*, or *constant*, or *floor* term and is depends on calibration uncertainties, detector non-uniformities (e.g. irregularities in the lattice arrangement of the SciFi in the PSG matrix), detector aging and radiation damage of the active medium (SciFi in our case). Specifically, instrumental effects, such as signal dependence of which fibers are hit and where they are hit, need to be minimized. Fiber-to-fiber fluctuations (precisely which fibers are hit) in light yield and effects due to fiber attenuation length (where the fibers are hit) are the main sources of non-uniformities. The former becomes important when a small number of fibers is hit in a shower, as is the case for electromagnetic showers, where the number of fibers hit may be in the low hundred's. The latter is more important for hadronic shower detection [23].

At higher incident energies, the floor term becomes a significant fraction of the energy resolution, and therefore every effort must be expended to keep it at the level 1% or smaller. The initial analysis of beam test date from Hall-B pointed to a floor term of a few percent (see Fig. 11 below), although $\sim$1% is expected as a final result based on the experience from the KLOE calorimeter [9]. This effort is underway in a recent analysis where cosmic ray data are being used to fine tune the BCAL's ADC calibration constants [31].

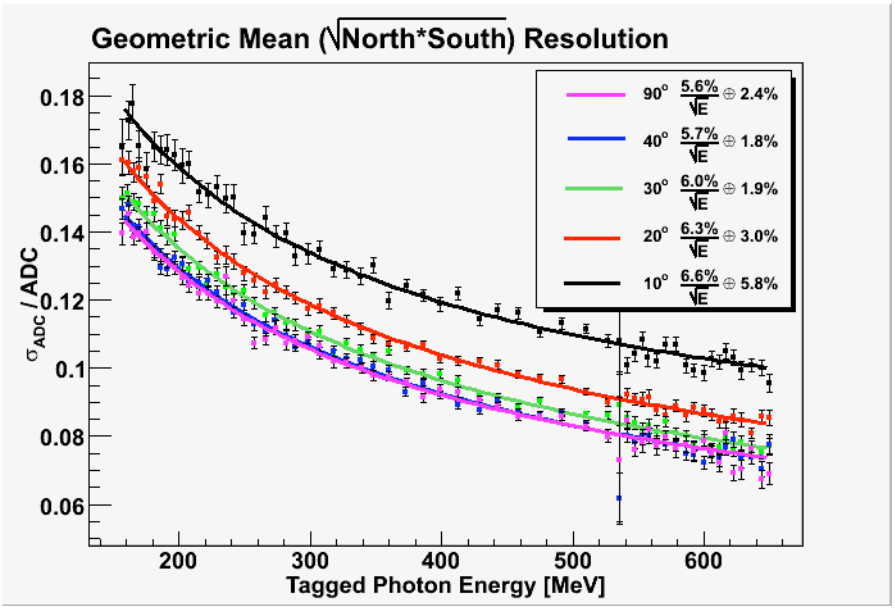

Fig. 12. BCAL single module energy resolution as a function of tagger energy for several incident photon angles, extracted from the Fall 2006 Beam Test data taken at Hall-B/Jefferson Lab [30].

6.1.3 Noise Term

Term c in Eq. (26) is known as the *noise* term and is due to electronic noise of the readout chain summed over readout channels within a few Molière radii. Calorimeters that have photosensitive readout (e.g. PMT or SiPM), which provides a high-gain multiplication of the original signal with little noise, enjoy a negligible noise term; this is the case for BCAL and justifies the omission of the noise term from fits such as those presented in Figs. 11 ans 12. Clearly, an increase in the sampling fraction of a calorimeter would offer a higher signal-to-noise ratio and a further suppression of the noise term.

6.1.4 Additional Contributions

When a calorimeter is integrated into an experiment additional contributions to the energy resolution may arise. These are itemized below, in the context of the BCAL and GlueX.

- *Longitudinal Leakage*: The dimensions of the inner tracking package (CDC, cylindrical drift chamber) and the inner bore of the super-conducting solenoid, restrict the BCAL total calorimeter thickness to 22.5 cm, or $15.5X_0$ at normal incidence, as shown in Table 6. It should be noted that most of the photon showers have angles in the forward region, thus resulting in much larger effective radiation lengths, reaching a peak value of $67X_0$ at $\theta = 15^o$, which is in the direction from the center of the target to the back corner of

the BCAL in the forward region. Furthermore, as shown in Fig. 8, a few percent of the shower's energy is lost through the rear of the calorimeter. More importantly, this leakage fluctuates on an event-by-event basis, thus deteriorating the energy resolution. This effect can be rectified, to a certain extend, by weighting the energy deposited by the showers in the last readout segments of a longitudinally segmented calorimeter [24].

- *Lateral Leakage*: Geometrical lateral leakage is not an issue for the BCAL, since its 48 modules will be mounted size by side, forming its barrel shape. However, in order to achieve a certain granularity in the readout of the device and to also limit the contribution to electronic noise from readout cells that do not fire for a given event, the cluster size used to reconstruct a shower may be limited. As a result, some of the shower's energy may not be properly accounted, and, again, this fluctuates event by event and degrades the energy resolution.
- *Upstream Losses*: This refers to losses due to materials in front of the BCAL, such as experimental target, start counter, CDC and FDC (Forward Drift Chambers), as well as associated mechanical structures and cables. For details on these materials the reader is referred to reference [32].
- *Non-hermetic Coverage*: Cracks and dead regions are expected along the 'seams' of the BCAL, where one module abuts its neighbor. The energy resolution is degraded for showers developing along these regions, and low-energy tails appear in the reconstructed energy spectra. Furthermore, the transverse energy of momentum measurement is affected. These seams have contributions from gaps due to machining imperfections that result in damaged fibers that are sheered to achieve the trapezoidal shape of each module, and possibly due to the addition of aluminum tape wrapped around each module at various places along its length, to assist its structural integrity and help prevent delamination. Detailed simulations of these will be performed in the future, when machining tolerances become known.

6.2 Timing and Position Resolution

Calorimeters based on scintillation light are quite fast in terms of timing. Fluctuations in photomultiplier transit time contribute a few nanoseconds to the signal width. Ultimately, the signal duration depends on the physics of the shower's development [23].

The timing difference resolution depends on the effective Molière radius and the transverse granularity of the calorimeter. It can be expressed as:

$$\sigma_t = \frac{d}{\sqrt{E}} \oplus e \tag{32}$$

A preliminary analysis of beam test data has yielded $d = 74$ ps and $e = 33$ ps for the time difference resolution (tagger independent quantity) and $d = 34$ ps and $e = 210$ ps for the mean timer resolution (tagger dependent quantity, prior to any tagger corrections) [30], that compare favorably to the respective numbers of $d = 54$ ps and $e = 140$ ps from KLOE [9]. See Figs. 13 and 14 for the relevant plots.

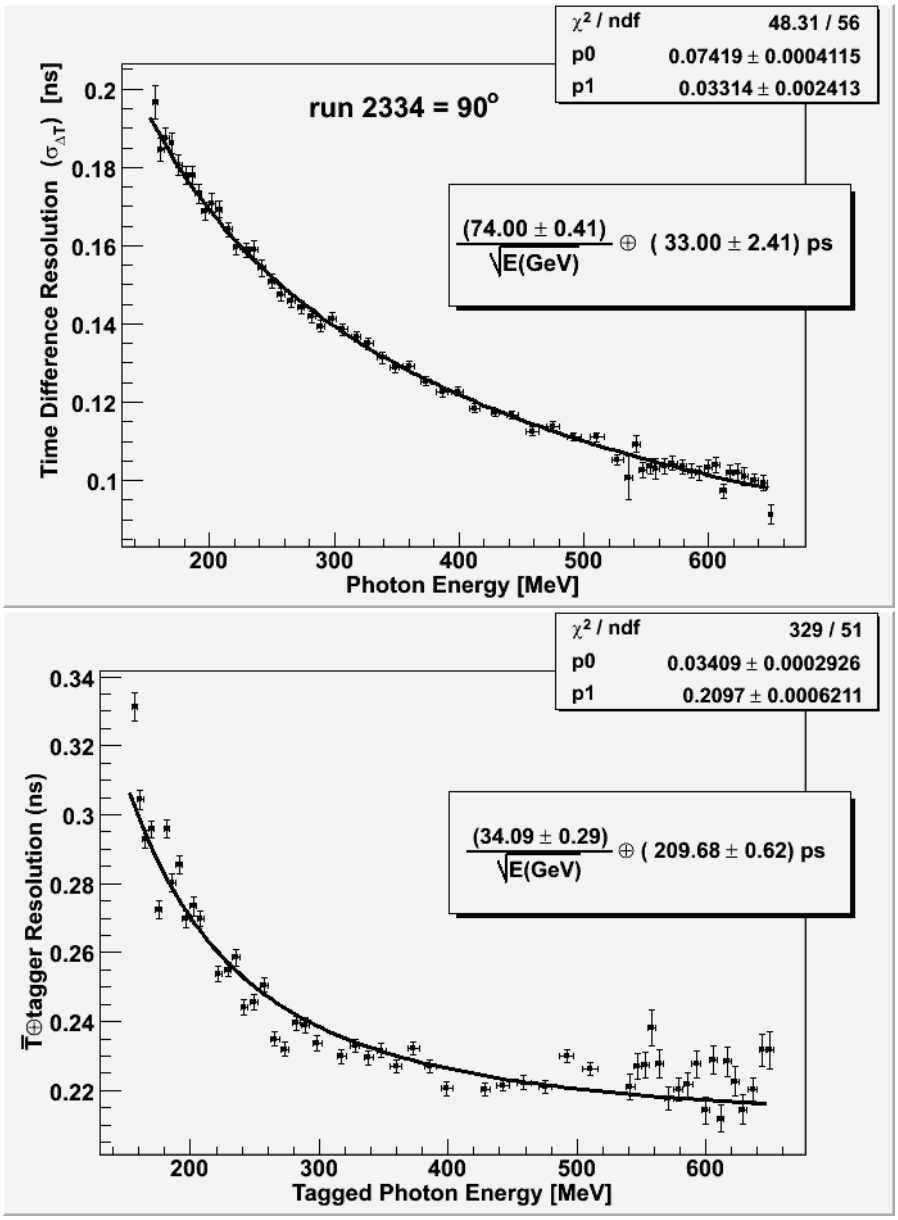

Fig. 13. Preliminary BCAL timing resolution of the difference between two ends (top panel) and of the mean of two ends as a function of tagger energy (bottom panel), extracted from the Fall 2006 Beam Test data taken at Hall-B/Jeffesron Lab [30].

Finally, based on experience from the JETSET PbSciFi calorimeter [33], a weighted position resolution of 5 mm/$\sqrt{E}$ can be expected: this leads to an azimuthal resolution for the BCAL of ~ 8.5 mrad. Finally, using the z-position

resolution of 2.5 cm as obtained from the above timing resolution ($\sim$ 150 ps) at 1 GeV, one obtains a polar angular resolution of $\sim$ 20 mrad at $\theta = 45^o$, using the following trigonometric equation, derived using the law of sines:

$$\sin(\delta\theta) = \frac{\delta z}{r}\sin^2\theta \Rightarrow \delta\theta \simeq \frac{\delta z}{r}\sin^2\theta \tag{33}$$

where r is the inner radius of the BCAL.

7 Summary of BCAL Properties

The properties and features of the BCAL are summarized in Table 9.

8 Conclusions

Analytical calculations were carried out in order to determine the calorimetry response of the BCAL electromagnetic calorimeter for the GlueX project, based on measurements of the volume ratios of lead, scintillating fibers and optical epoxy, as well as knowing the chemical composition of these materials from their manufacturer. The summary of all properties is shown in Table 9.

Among these, the radiation length was determined to be 1.46 cm, the critical energy is 8.4 MeV, and the Molière radius is 3.63 cm, all based on the calculated, effective mass number, atomic number and density of 179.9, 71.37 and 4.88 g/cm^3.

The analytical shower depth profile as well as the small amount of energy leaking through the rear of the BCAL ($t_{95\%} \sim 20X_0$) are in agreement with recent Monte Carlo simulations [20]. The latter number demonstrates that the design thickness of the BCAL is more than adequate to collect the majority of the em shower, thus achieving a primary design goal of efficiently containing showers in forward angles up to normal incidence. The former shows that most of the secondaries and deposited energy occur in the first 8$-$10 cm and it is there where higher readout sampling, resolution and better timing characteristics are required. The readout requirements for the remainder of the depth can be somewhat more relaxed.

This work was supported in part by NSERC (Canada) and Jefferson Lab (USA). The Southeastern University Research Association (SURA) operates the Thomas Jefferson National Accelerator Facility for the U.S. Department of Energy under contract DE-AC05-84ER40150.

Property	**Symbol**	**Value**
Module Length	L	390 cm
Module Inner Cord	c_i	8.51 cm
Module Outer Cord	c_o	11.77 cm
Module Thickness	d	22.5 cm
Module Azimuthal Bite	$\Delta\phi$	7.5^o
Radial Fiber Pitch	p_r	1.18 mm
Azimuthal Fiber Pitch	p_ϕ	1.35 mm
Volume Ratios	Pb:SciFi:Glue	37:49:14
Effective Mass Number	A_{eff}	179.9
Effective Atomic Number	Z_{eff}	71.4
Effective Density	ρ_{eff}	4.88 g/cm^3
Critical Energy	E_c	11.02 MeV [17], 8.36 MeV [18]
Radiation Length	X_0	7.06 g/cm^2 or 1.45 cm
No of Radiation Lengths	nX_0	$15.5X_0$ (at normal incidence)
Max Shower	t_{max}	$5.0X_0$ [17], $5.3X_0$ [18] (at 1 GeV)
95% Shower	$t_{95\%}$	$20.3X_0$ [17], $20.6X_0$ [18] (at 1 GeV)
Molière Radius	R_M	17.7 g/cm^2 or 3.63 cm [18]
Energy Resolution	$\frac{\sigma_E}{E}$	$5\%/\sqrt{E} \oplus 1\%$
Timing Difference Resolution	σ_{TDIF}	74 ps$/\sqrt{E} \oplus$ 33 ps
Mean Timer Resolution	σ_{MT}	34 ps$/\sqrt{E} \oplus$ 210 ps
Position Resolution	σ_{pos}	5 mm$/\sqrt{E}$ (weighted)
Azimuthal Resolution	σ_ϕ	$\sim$ 8.5 mrad
Polar Resolution	σ_θ	$\sim$ 20 mrad (at $\theta = 45^o$)

Table 9
List of the BCAL's properties and features.

References

[1] GlueX/Hall D Collaboration, The Science of Quark Confinement and Gluonic Excitations, GlueX/Hall D Design Report, **Ver.4** (2002).
http : *//www.phys.cmu.edu/halld.*

[2] A.R. Dzierba, C.A. Meyer and E.S. Swanson, American Scientist, **88**, 406 (2000).

[3] G.J. Lolos, Eur. Phys. J. A **17**, 499 (2002).

[4] Z. Papandreou, R. Hakobyan and N. Kolev, GlueX-doc-439 (2005).

[5] Review of Particle Physics, Phys. Rev. D **66** 010001-199 (2002).

[6] Wikipedia, http://en.wikipedia.org/wiki/Polystyrene.

[7] St. Gobain Crystals, SGC Scintillating Optical Fibers Brochure 605.

[8] K. Janzen and C. Ingram, private communication, University of Regina (2007).

[9] M. Adinolfi *et al.*, NIM A **482**, 364 (2002).

[10] Y.S. Tsai, Rev. Mod. Phys. **46**, 815 (1974).

[11] O.I. Dahl, private communication with PDG.

[12] D.H. Perkins, *Introduction to High Energy Physics*, Second Edition, Addison-Wesley Publishing Company, Inc., (1982).

[13] Electron Gamma Shower Package EGS5, SLAC Note SLAC-R-730 (2005).

[14] GEANT 3.16 Manual, CERN Program Library Long Writeup W5013 (1994).

[15] H. Davies, H.A. Bethe, and L.C. Maximon, Phys, Rev. **93**, 788 (1954).

[16] Grapher, Version 1.0, Apple Computer Inc., (2005).

[17] M.J. Berger and S.M. Seltzer, "Tables of Energy Losses and Ranges of Electrons and Positrons," National Aeronautics and Space Administration Report NASA-SP-3012, Washington, DC (1964).

[18] B. Rossi, *High Energy Particles*, Prentice-Hall, Inc., Engelwood Cliffs, NJ (1952).

[19] IGOR Pro, Version 6.0, WaveMetrics, Inc., (2007).

[20] R. Hakobyan and Z. Papandreou, GlueX-doc-829 (2007).

[21] S. Katsaganis, "BCAL and Tungsten", GlueX-doc-841 (2005).

[22] G. Bathow *et al.*, Nucl. Phys. **B20**, 259 (1970).

[23] M. Livan, V. Vercesi and R. Wigmans, "Scintillating-Fibre Calorimetry", CERN-95-02 (1995).

[24] C.W. Fabjan and F. Gianotti, "Calorimetry for Particle Physics", CERN-EP/2003-075 (2003).

[25] R.T Jones. "Uniformity Requirements for the GlueX Barrel Calorimeter", GlueX-doc-812 (2007).

[26] U. Amaldi, Phys. Scr. **23**, 409 (1981).

[27] R. Wigmans, Nucl. Instr. and Meth. **A259**, 389 (1987).

[28] B. Leverington, "Sampling Fraction Fluctuations", GlueX-doc-827 (2007).

[29] E.S. Smith, "Specification and Evaluation of BCAL Readout Options", GlueX-doc-795 (2007).

[30] B. Leverington, "Analysis of the BCAL Hall-B Beam test", GlueX-doc-804 (2007).

[31] A.R. Dzierba, "Calibrating BCAL with Cosmic Rays", GlueX-doc-834 (2007).

[32] R.T Jones. "Discussion of the Detector Material Budget", GlueX-doc-789 (2007).

[33] D. Hertzog et al., Nucl. Instr. and Meth. **A294**, 446 (1990).